Electronic Supplementary Material (ESI) for Physical Chemistry Chemical Physics.

Supplementary Information : Multi-Layer Energy-Based Fragment Method for Excited States and Nonadiabatic Dynamics

Wen-Kai Chen, Wei-Hai Fang, and Ganglong Cui*

Key Laboratory of Theoretical and Computational Photochemistry, Ministry of Education, College of Chemistry, Beijing Normal University, Beijing 100875, China

Email: ganglong.cui@bnu.edu.cn

Contents

1 Computational Methods

In this work we have used 200 structures of $CH_3N{=}NCH_3$-$(H_2O)_5$ as benchmark data sets. These 200 structures are randomly selected from a 2 ps canonical molecular dynamics trajectory at BP86/def2-SVP level.[1–3] Time step of 1 fs is used for nuclear propagation and five-order Nosé-Hoover chain thermostat technique is used to control temperature in NVT molecular dynamics simulations (300K). MD is performed using Chemshell3.5[4] interfaced with Turbomole6.6.[5]

In our calculations B3LYP method[2,6–8] is used for the outer region while CASSCF is selected for the inner region. For both DFT and CASSCF calculations, we have used 6-31+G** basis set.[9–12] We have used state-averaged (SA)-CASSCF method with an active space of six electrons in four orbitals, denoted CASSCF(6,4), which contains π and π^* orbitals of N=N and two lone-pair orbitals on two nitrogen atoms.[13–15] This active space can be maintained through reading a pre-generated active space. All B3LYP calculations are done with Gaussian16[16] and all CASSCF calculations are performed with MOLCAS8.0.[17,18]

2 Zhu-Nakamura Non-Adiabatic Dynamics Method

Trajectory-based surface hopping methods are one of popular methods that perform nonadiabatic dynamics simulations. In dynamics simulations, the system is propagated in an electronic state but can jump to other potential energy surfaces in particular near quasi-degenerate regions. In this work, we have used Zhu-Nakamura method to compute transition probabilities among different potential energy surfaces. This method is developed by Zhu et al.[19–21] and is able to calculate nonadiabatic transition probabilities,

$$p = exp\left[-\left(\frac{\pi}{4\sqrt{a^2}}\sqrt{\frac{2}{b^2+\sqrt{|b^4\pm 1|}}}\right)\right], \tag{S1}$$

in which a and b are two unitless parameters, i.e., effective coupling and collision energy, which are written as

$$a^2 = \frac{\hbar^2}{2\mu}\frac{\sqrt{|F_1F_2|}|F_2-F_1|}{(2V_{12})^3} \tag{S2}$$

and

$$b^2 = (E_t - E_x)\frac{|F_2 - F_1|}{\sqrt{|F_2F_1|}(2V_{12})}, \tag{S3}$$

where F_1 and F_2 are two mass-scaled one-dimensional diabatic forces, μ is reduced mass of the diabatic molecule, V_{12} is diabatic coupling, E_x is the energy at crossing point, E_t is potential energy plus kinetic energy component along hopping vector direction. Finally, mass-scaled one-dimensional diabatic forces in Eqs. S2 and S3 are converted from mass-scaled multidimensional diabatic forces based on

$$\frac{\sqrt{|F_2F_1|}}{\sqrt{\mu}} = \sqrt{\left|\sum_{i=1}^{N}\frac{1}{m_i}\sum_{\alpha=x,y,z}F_2^{i\alpha}F_1^{i\alpha}\right|} \tag{S4}$$

and

$$\frac{|F_2 - F_1|}{\sqrt{\mu}} = \sqrt{\sum_{i=1}^{N}\frac{1}{m_i}\sum_{\alpha=x,y,z}\left(F_2^{i\alpha} - F_1^{i\alpha}\right)^2}, \tag{S5}$$

in which N is the number of atoms in a system; m_i is the mass of the ith atom; $F_1^{i\alpha}$ and $F_2^{i\alpha}$ are multi-dimensional diabatic forces of the ith atom (α :, x, y, and z) related to involved two states. These diabatic forces can be further converted from multi-dimensional adiabatic forces, which are directly calculated by external electronic structure packages. The detailed description can be found in recent works by Zhu and co-workers.[22,23] The advantage of Zhu–Nakamura method compared with other surface-hopping methods is that it does not need to compute nonadiabatic coupling vectors.

Initial conditions of non-adiabatic molecular dynamics simulations are sampled via Wigner sampling, which is performed by Newton-X.[24–27] In order to make comparison between CASSCF with MLEBF method, same initial conditions are used in both kinds of dynamics simulations. For each trajectory, 500 fs propagation time with 0.5 fs time step are carried out using our GTSH package.[28]

3 Additional Results for MLEBF Method Truncated at Second Order

Dynamical results of both ab initio- and MLEBF-based nonadiabatic dynamics simulations are pretty similar to each other. In addition to those discussed already in the main text, the following results are also discussed here. The distribution of the C3N2N1C7 dihedral angle at the hopping points (Fig. S2) is very similar for both ab initio-

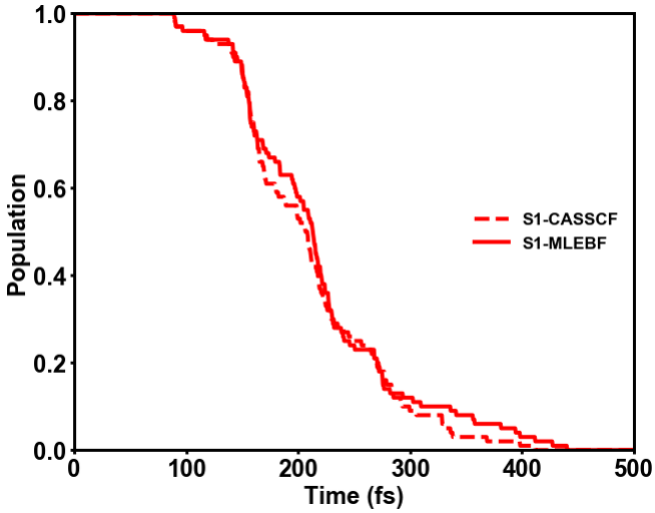

Figure S1: Time-dependent S_1 state population in full CASSCF- and MLEBF-based dynamics simulations.

and MLEBF-based dynamics simulations. Fig. S1 shows time-dependent S_0 and S_1 state populations averaged over 100 trajectories. Their time evolution is also very similar for both CASSCF and MLEBF dynamics. The small deviation of MLEBF populations from ab initio ones is observed and is the inevitable result of non-negligible albeit tiny deviation between MLEBF and ab initio energies and forces. Nevertheless, the MLEBF method still give accurate S_0 and S_1 state populations. Fig. S3 shows the distribution of S_0-S_1 energy gaps of 100 trajectories in the Franck–Condon region, i.e., vertical excitation energies. The MLEBF methods reproduce closely vertical excitation energies calculated at CASSCF level. In both ab initio and MLEBF cases, the same distribution width, ranging from 3.3 to 4.3 eV, and the same peak at 3.7 eV are observed.

Additionally, whether total energy is conserved or not in dynamics simulation is very important for MLEBF method. In principle, molecular dynamics simulations should have conserved total energy if energies and forces are highly accurate. In MLEBF method, the total energy is conserved well compared with those based on full ab initio ones (see Fig. S4).

For our system, without breaking chemical bonds, we have therefore tested the effects of different active spaces on the results. The MLEBF calculations with CASSCF(2,2) for the photochemically active region give similarly accurate results with those with CASSCF(6,4). With CASSCF(2,2), RMSD values of S_0 and S_1 energies are 1.90×10^{-2} and 1.89×10^{-2} eV/fragment and those of the corresponding gradients are 1.13×10^{-2} and 1.13×10^{-2} eV/Å when truncated at the two-body interaction with the electrostatically embedding. The corresponding excitation energies are also precise with RMSD of 2.66×10^{-3} eV (see Fig. S6).

In our present MLEBF calculations we have used CASSCF for the interlayer interaction as we need to explicitly

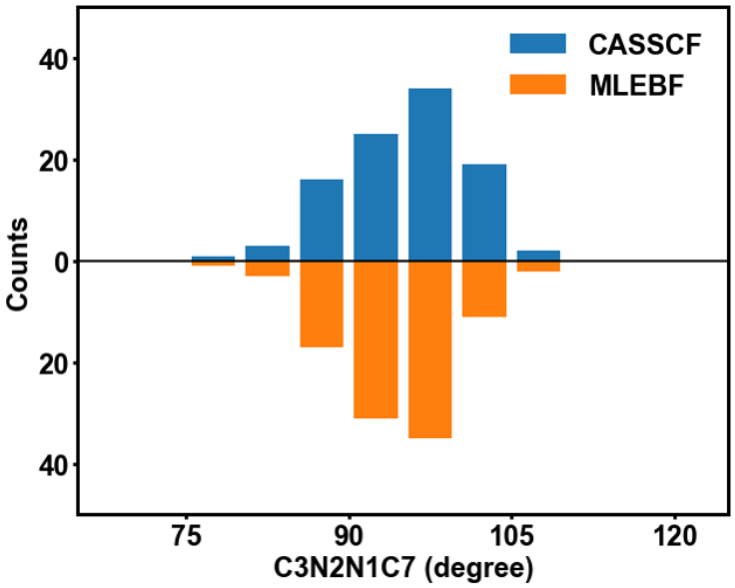

Figure S2: Distribution of the dihedral angle C3N2N1C7 at the hopping points based on (up) CASSCF method and (down) MLEBF method. Both kinds of simulations give similar distribution.

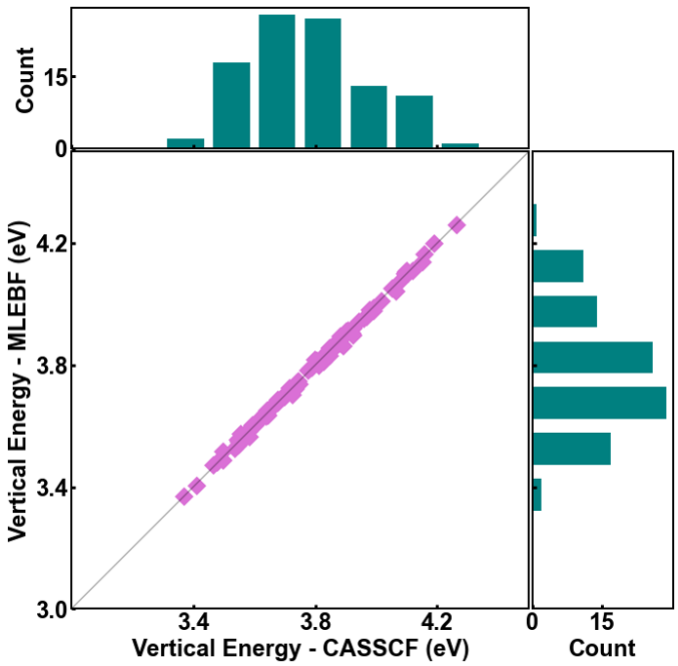

Figure S3: Comparison of the S_0-S_1 energy gap (eV) of 100 trajectories at the starting points calculated with full CASSCF and MLEBF methods.

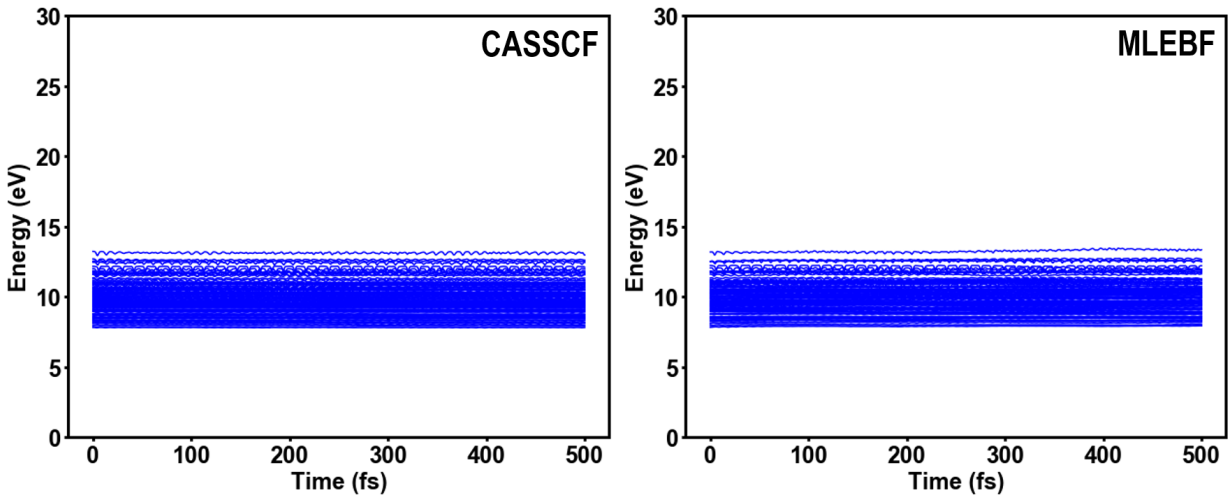

Figure S4: Time-dependent evolution of total energy of all trajectories in (left) CASSCF- and (right) MLEBF-based MD simulations.

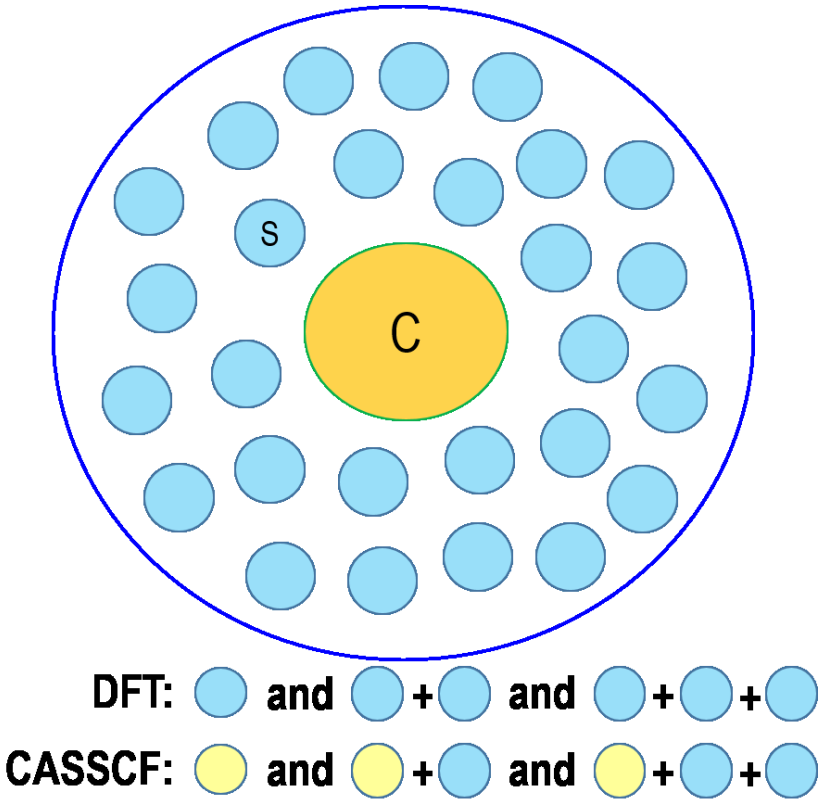

Figure S5: Two-layer model of the developed multi-layer energy-based fragment (MLEBF) method truncated at the third order.

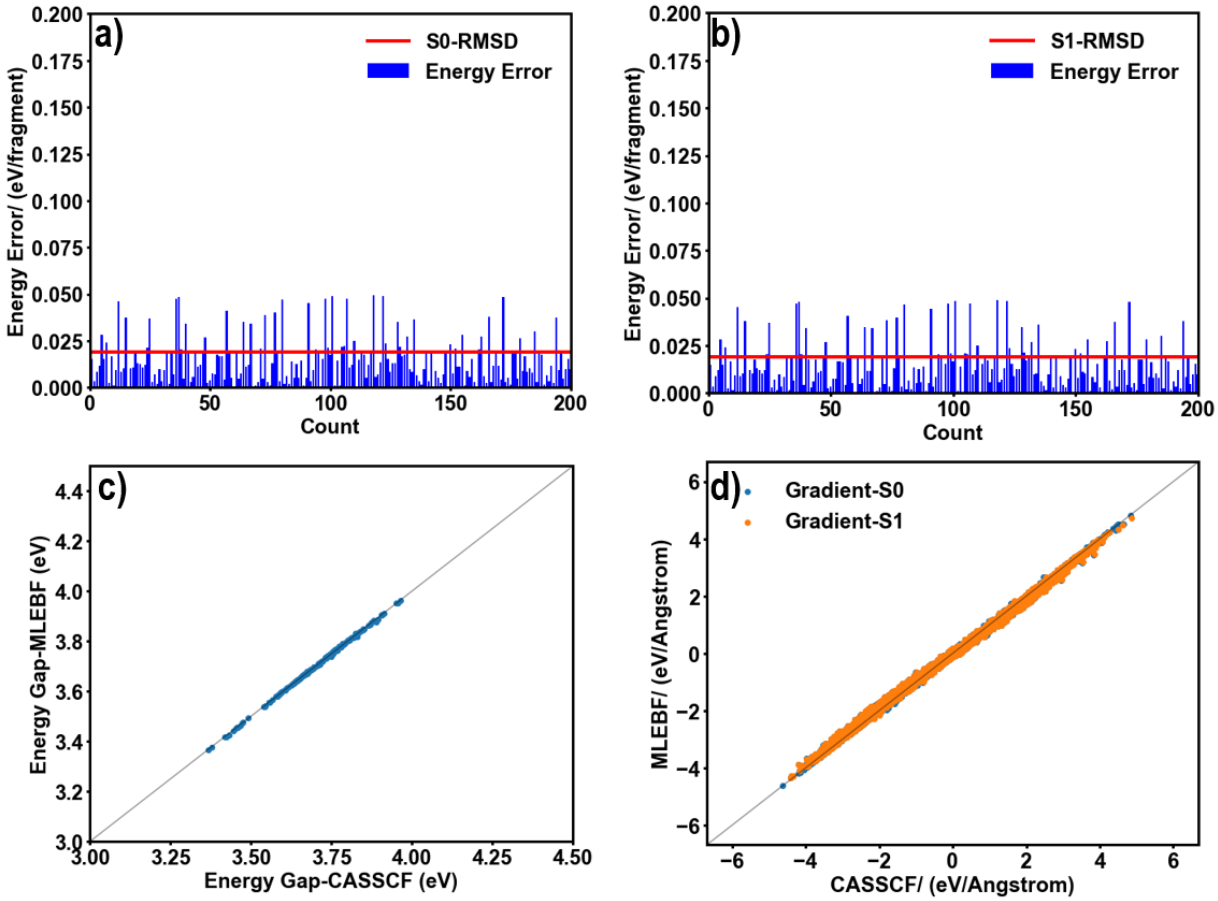

Figure S6: Comparison of both S_0 and S_1 energies (top), energy gaps (bottom-left), and both S_0 and S_1 gradients (bottom-right) calculated using EE-MLEBF-2nd truncated at the two-body interaction level. The CAS(2,2) method is used for the intralayer interaction of the inner region and the interlayer interaction between the inner and outer regions.

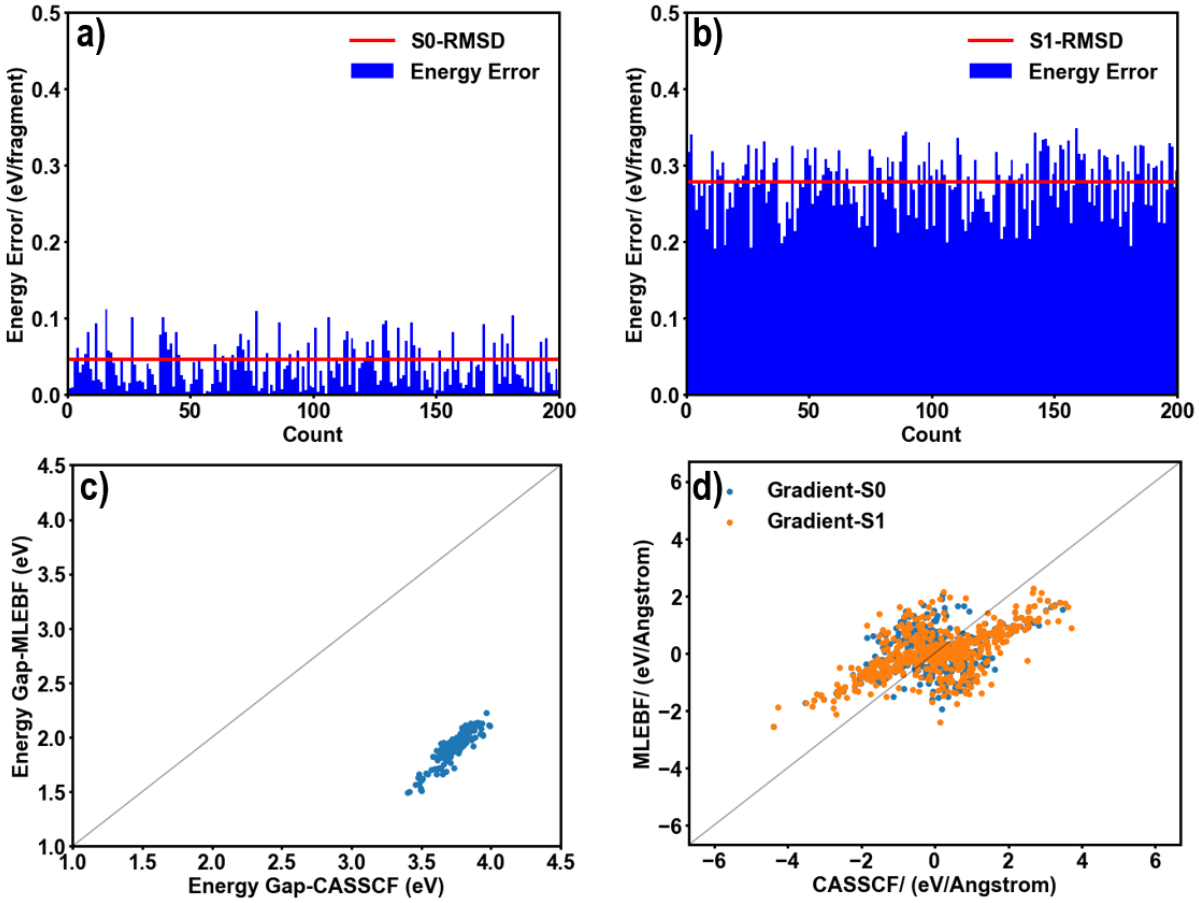

Figure S7: Comparison of both S_0 and S_1 energies (top), energy gaps (bottom-left), and both S_0 and S_1 gradients (bottom-right) calculated using EE-MLEBF-2nd truncated at the two-body interaction level. The CASSCF method is used for the intralayer interaction of the inner region; but, the interlayer interaction between the inner and outer regions is calculated with DFT.

calculate state-specific polarization effects of the outer region on the inner region at least at the two-body interaction level. If using DFT, e.g. B3LYP/6-31+G** level, for the interlayer interaction, the results become much less accurate. For example, in ground state MLEBF calculations, if the interlayer dimers' energies and gradients are calculated with DFT and the intralayer interactions of the inner and outer layers are treated with CASSCF and DFT, RMSD of S0 energies is 4.59×10^{-2} eV/monomer, less accurate than those with CASSCF for the interlayer interaction (1.90×10^{-2} eV/monomer). More unfortunately, gradients become much worse and RMSD is 0.190 eV/Å. In comparison, either energies or gradients of the S_1 state become much worse compared with full CASSCF ones In addition, excitation energies are also not precise compared with full CASSCF calculations. Its RMSD is up to 1.8 eV.

The poor performance of DFT for the interlayer interaction is due to its inaccurate description (see Fig. S8). It can be found that for the S_0 state, DFT calculated interlayer interaction energies are not so worse compared with

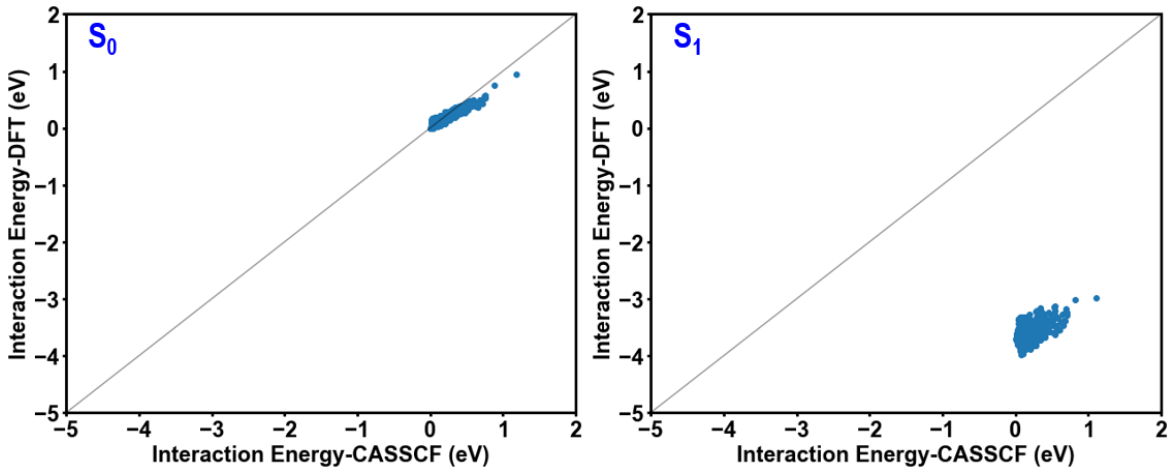

Figure S8: Comparison of both S_0 (left) and S_1 energies (right) calculated by EE-MLEBF-2nd in which DFT and CASSCF are employed for the interlayer interaction.

those with CASSCF, so that one can see "not-so-bad" S_0 energies in the top-left panel of Fig. S7. Of course, the S_0 gradients are really worse in the bottom-right panel of Fig. S7. But, for the S_1 state, DFT calculated interlayer interaction energies are far away from those with CASSCF (see the right panel of Fig. S8). As a result, bad S_1 energies and gradients are observed in the top-right and bottom-right panels of Fig. S7. Due to bad S_1 energies, it cannot be expected to give good S_0-S_1 energy gaps (see the bottom-left panel of Fig. S7).

4 MLEBF Method Truncated at Third Order

Total energy of a system consisting of N monomers, within many-body expansion (MBE) truncated at the third order is written as[29]

$$E = E(1) + E(2) + E(3) \tag{S6}$$

in which the first- , second-, and third-order energy terms are written as

$$E(1) = \sum_{i}^{N} E_i \tag{S7}$$

$$E(2) = \sum_{i<j}^{N} (E_{ij} - E_i - E_j) \tag{S8}$$

$$E(3) = \sum_{i<j<k}^{N} [(E_{ijk} - E_i - E_j - E_k) - (E_{ij} - E_i - E_j) - (E_{ik} - E_i - E_k) - (E_{jk} - E_j - E_k)] \tag{S9}$$

where E_i, E_{ij}, E_{ijk} are energies of monomers, dimers, and trimers embedded in the field of N-1, N-2, N-3 other particles.[29] So if only truncated at the third level, the total energy is approximately expressed as

$$E = \sum_{i<j<k}^{N} E_{ijk} - (N-3)\sum_{i<j}^{N} E_{ij} + \frac{(N-2)(N-3)}{2}\sum_{i}^{N} E_i \tag{S10}$$

If one calculates the energies using equation S10 without the presence of the point charges, then one gets the convetional three-body expansion energies.

Now we consider a three-order MLEBF method, which is similar to the two-order MLEBF discussed in the main text. The inner layer, called the active region, involves the region in which complicated chemical bonds' making and breaking, e.g. photoisomerization, take place. This region is described using CASSCF. By contrast, the outer region only undergoes conformational changes without involving chemical reactions; as a result, this region is treated with relatively efficient DFT. The interlayer interaction is also described by means of CASSCF in order to treat the polarization of the outer layer on the inner one at the same level as done for the inner region. With this two-layer model, Eq. S9 is re-written as:

$$E(3)_{MLEBF} = E(3)_{iii} + E(3)_{iio} + E(3)_{ioo} + E(3)_{ooo} \tag{S11}$$

in which the trimer energy $E(3)_{iii}$ with subscription *iii* means all monomers of the trimer are in the inner layer, subscription *ooo* means all monomers of the trimer are in the outer layer, subscription *ioo* means one monomer is in the inner layer while two monomers are in the outer layer, and subscription *iio* means two monomers are in the inner layer while one monomer is in the outer layer. As a result, these four terms in Eq. S11 becomes

$$E(3)_{iii} = \sum_{i<j<k}^{N_{in}} E_{ijk} - (N_{in}-2)\sum_{i<j}^{N_{in}} E_{ij} + \frac{(N_{in}-1)(N_{in}-2)}{2}\sum_{i}^{N_{in}} E_i \tag{S12}$$

$$E(3)_{iio} = \sum_{i<j}^{N_{in}}\sum_{k}^{N_{out}} E_{ijk} - (N_{in}-1)\sum_{i}^{N_{in}}\sum_{j}^{N_{out}} E_{ij} - N_{out}\sum_{i<j}^{N_{in}} E_{ij} + (N_{in}-1)N_{out}\sum_{i}^{N_{in}} E_i + \frac{(N_{in}-1)N_{in}}{2}\sum_{i}^{N_{out}} E_i \tag{S13}$$

$$E(3)_{ioo} = \sum_{i}^{N_{in}} \sum_{j<k}^{N_{out}} E_{ijk} - (N_{out}-1) \sum_{i}^{N_{in}} \sum_{j}^{N_{out}} E_{ij} - N_{in} \sum_{i<j}^{N_{out}} E_{ij} + \frac{(N_{out}-1)N_{out}}{2} \sum_{i}^{N_{in}} E_i + N_{in}(N_{out}-1) \sum_{i}^{N_{out}} E_i \quad \text{(S14)}$$

$$E(3)_{ooo} = \sum_{i<j<k}^{N_{out}} E_{ijk} - (N_{out}-2) \sum_{i<j}^{N_{out}} E_{ij} + \frac{(N_{out}-1)(N_{out}-2)}{2} \sum_{i}^{N_{out}} E_i \quad \text{(S15)}$$

In Eqs. S12-S15, N_{in} and N_{out} represent the numbers of monomers in both inner and outer layers, respectively. Inserting Eqs. S12-S15 into Eq. S11 and considering $N = N_{in} + N_{out}$, it is also expressed

$$\begin{aligned} E(3)_{MLEBF} = \quad & \sum_{i<j<k}^{N_{in}} E_{ijk} + \sum_{i<j}^{N_{in}} \sum_{k}^{N_{out}} E_{ijk} + \sum_{i}^{N_{in}} \sum_{j<k}^{N_{out}} E_{ijk} + \sum_{i<j<k}^{N_{out}} E_{ijk} \\ & -(N-2)\Big(\sum_{i<j}^{N_{in}} E_{ij} + \sum_{i}^{N_{in}} \sum_{j}^{N_{out}} E_{ij} + \sum_{i<j}^{N_{out}} E_{ij} \Big) \\ & + \frac{(N-1)(N-2)}{2} \Big(\sum_{i}^{N_{in}} E_i + \sum_{i}^{N_{out}} E_i \Big) \end{aligned} \quad \text{(S16)}$$

Integrating Eq. S16 and Eq. 5 in the main text, Eq. S10 is re-written as:

$$\begin{aligned} E = \quad & \sum_{i<j<k}^{N_{in}} E_{ijk} + \sum_{i<j}^{N_{in}} \sum_{k}^{N_{out}} E_{ijk} + \sum_{i}^{N_{in}} \sum_{j<k}^{N_{out}} E_{ijk} \\ & -(N-3) \sum_{i<j}^{N_{in}} E_{ij} - (N-3) \sum_{i}^{N_{in}} \sum_{j}^{N_{out}} E_{ij} + \frac{(N-2)(N-3)}{2} \sum_{i}^{N_{in}} E_i \\ & + \sum_{i<j<k}^{N_{out}} E_{ijk} - (N-3) \sum_{i<j}^{N_{out}} E_{ij} + \frac{(N-2)(N-3)}{2} \sum_{i}^{N_{out}} E_i \end{aligned} \quad \text{(S17)}$$

in which only the first six terms are described with CASSCF and the latter three terms are treated with efficient DFT (see Fig. S5). In realistic applications, if only one chromophore is included in the inner region, the first, second, and fourth terms disappear and the third, fifth, and sixth terms are signifcantly reduced. It should be stressed that in the current implementation we did not calculate the gradients of the embedding point charges, which could be considered in future.

5 Results of MLEBF Truncated at Third Order

As mentioned in the main text, adding the three-body term in MLEBF method decreases errors roughly by an order of magnitude. Here, we have tested conventional (No-EE-MLEBF-3rd) and eletrostatically embedding

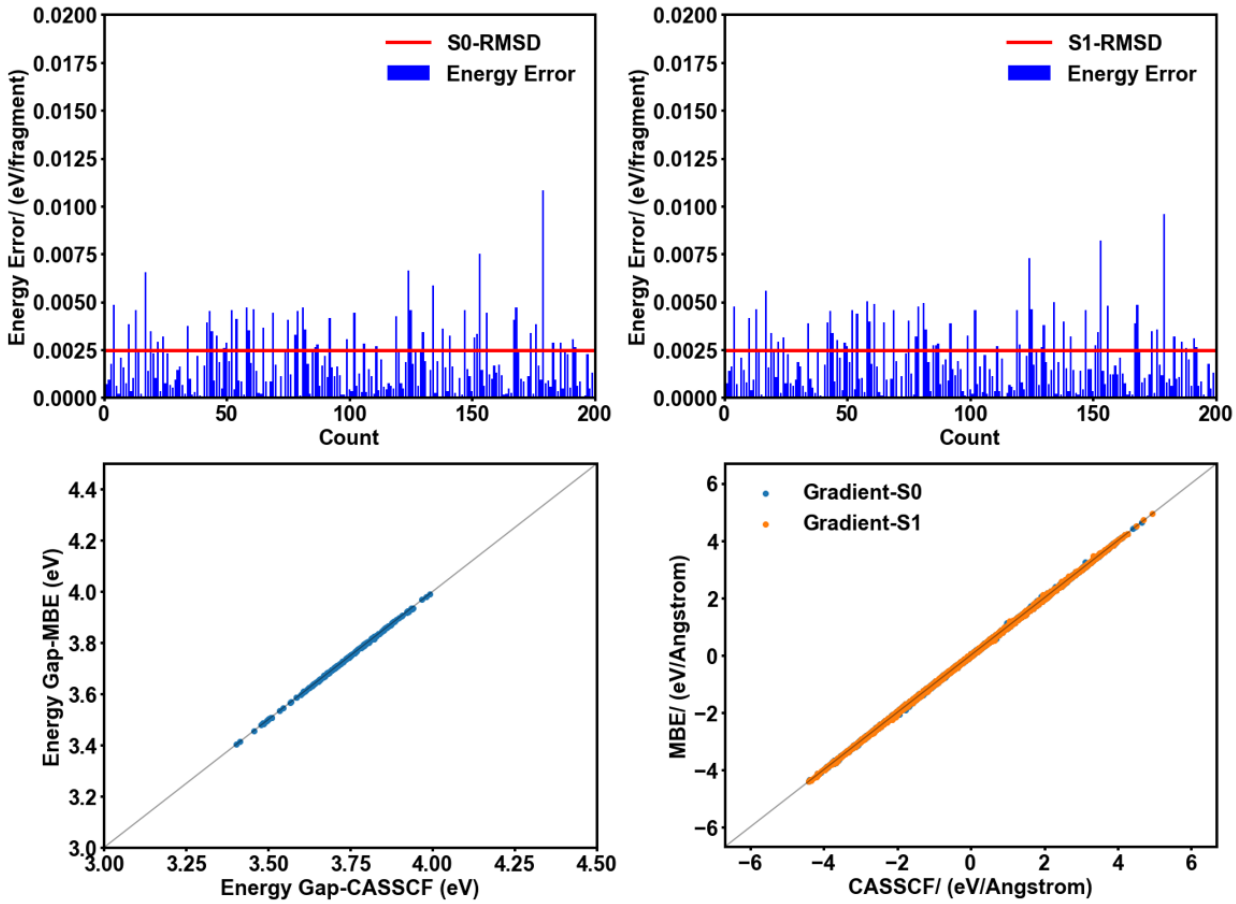

Figure S9: Comparison of both S_0 and S_1 energies (top-left and -right), energy gaps (bottom-left), and both S_0 and S_1 gradients (bottom-right) calculated using No-EE-MLEBF-3rd truncated at the three order interaction, and full CASSCF methods.

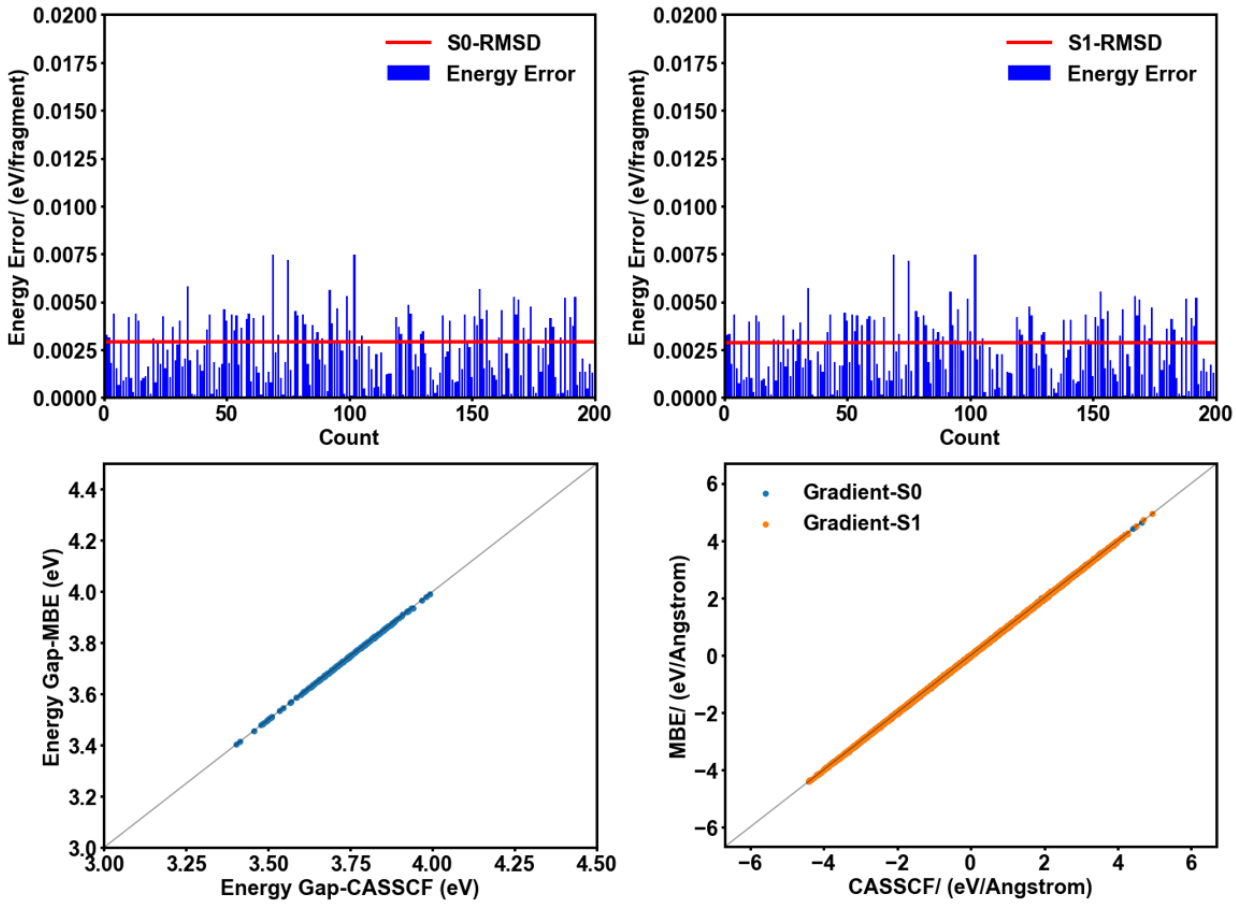

Figure S10: Comparison of both S_0 and S_1 energies (top-left and -right), energy gaps (bottom-left), and both S_0 and S_1 gradients (bottom-right) calculated using EE-MLEBF-3rd truncated at the three order interaction, and full CASSCF methods.

(EE-MLEBF-3rd) three-order MLEBF method. Both No-EE- and EE-MLEBF-3rd are much more accurate than the two-order EE-MLEBF results (See Figs. S9 and S10, and Table S1).

6 Speedup of MLEBF

Like other energy-based fragment methods, as mentioned in the main text, our MLEBF method is also highly parallel. Thus, we have also calculated different CPU times for single-point energies of two different systems (see table S2). For 1 CPU calculations, EE-2B-MLEBF is faster than CASSCF, which becomes more obvious with $CH_3N{=}NCH_3$-$(H_2O)_{20}$ (more than 20 times). When adding the three-body interaction, EE-3B-MLEBF remains comparable with CASSCF; however, it should become much more efficient with larger systems. In addition, it is also clear that parallelization will significantly speedup MLEBF calculations, which cannot be

Table S1: Root Mean Square Deviation (RMSD) Errors of Energies (eV/monomer) and Gradients (eV/Å) between EE-MLEBF-2nd, No-EE-MLEBF-3rd, and EE-MLEBF-3rd Methods in Comparison with Full CASSCF Calculations.

	Energies (S_0)	Energies (S_1)	Gradients (S_0)	Gradients (S_1)
EE-MLEBF-2nd	$1.90 * 10^{-2}$	$1.88 * 10^{-2}$	$1.13 * 10^{-2}$	$1.14 * 10^{-2}$
No-EE-MLEBF-3rd	$2.45 * 10^{-3}$	$2.47 * 10^{-3}$	$1.91 * 10^{-3}$	$1.86 * 10^{-3}$
EE-MLEBF-3rd	$2.89 * 10^{-3}$	$2.87 * 10^{-3}$	$1.13 * 10^{-3}$	$1.11 * 10^{-3}$

Table S2: Times used in EE-2B-MLEBF, EE-3B-MLEBF, and full CASSCF single-point calculations for two large systems with different CPU numbers

	$CH_3N{=}NCH_3{-}(H_2O)_{10}$	$CH_3N{=}NCH_3{-}(H_2O)_{20}$
EE-2B-MLEBF (10 CPU)	9.90×10^1 s	2.58×10^2 s
EE-2B-MLEBF (1 CPU)	9.79×10^2 s	2.47×10^3 s
EE-3B-MLEBF (10 CPU)	1.01×10^3 s	3.41×10^3 s
EE-3B-MLEBF (1 CPU)	9.77×10^3 s	3.29×10^4 s
Full CASSCF	2.75×10^3 s	4.32×10^4 s

realized by full CASSCF calculations.

References

(1) J. P. Perdew, *Phys. Rev. B*, 1986, **33**, 8822–8824.

(2) A. D. Becke, *Phys. Rev. A*, 1988, **38**, 3098–3100.

(3) F. Weigend and R. Ahlrichs, *Phys. Chem. Chem. Phys.*, 2005, **7**, 3297–3305.

(4) *ChemShell3.5, a Computational Chemistry Shell, see www.chemshell.org*.

(5) *TURBOMOLE V6.6, 2014, a development of University of Karlsruhe and Forschungszentrum Karlsruhe GmbH, 1989-2007,TURBOMOLE GmbH, since 2007; available from* `http://www.turbomole.com`.

(6) C. Lee, W. Yang and R. G. Parr, *Phys. Rev. B*, 1988, **37**, 785.

(7) S. H. Vosko, L. Wilk and M. Nusair, *Can. J. Phys.*, 1980, **58**, 1200–1211.

(8) P. J. Stephens, F. J. Devlin, C. F. N. Chabalowski and M. J. Frisch, *J. Phys. Chem.*, 1994, **98**, 11623–11627.

(9) R. Ditchfield, W. J. Hehre and J. A. Pople, *J. Chem. Phys.*, 1971, **54**, 724–728.

(10) W. J. Hehre, R. Ditchfield and J. A. Pople, *J. Chem. Phys.*, 1972, **56**, 2257–2261.

(11) P. C. Hariharan and J. A. Pople, *Theor. Chim. Acta*, 1973, **28**, 213–222.

(12) T. Clark, J. Chandrasekhar, G. W. Spitznagel and P. V. R. Schleyer, *J. Comput. Chem.*, 1983, **4**, 294–301.

(13) B. Sellner, M. Ruckenbauer, I. Stambolić, M. Barbatti, A. J. A. Aquino and H. Lischka, *J. Phys. Chem. A*, 2010, **114**, 8778–8785.

(14) M. Ruckenbauer, M. Barbatti, B. Sellner, T. Muller and H. Lischka, *J. Phys. Chem. A*, 2010, **114**, 12585–12590.

(15) A. Gaenko, A. DeFusco, S. A. Varganov, T. J. Martínez and M. S. Gordon, *J. Phys. Chem. A*, 2014, **118**, 10902–10908.

(16) M. Frisch, G. Trucks, H. Schlegel, G. Scuseria, M. Robb, J. R. Cheeseman, G. Scalmani, V. Barone, G. Petersson, H. Nakatsuji, X. Li, M. Caricato, A. V. Marenich, J. Bloino, B. G. Janesko, R. Gomperts, B. Mennucci, H. P. Hratchian, J. V. Ortiz, A. F. Izmaylov, J. L. Sonnenberg, D. Williams-Young, F. Ding, F. Lipparini, F. Egidi, J. Goings, B. Peng, A. Petrone, T. Henderson, D. Ranasinghe, V. G. Zakrzewski,

J. Gao, N. Rega, G. Zheng, W. Liang, M. Hada, M. Ehara, K. Toyota, R. Fukuda, J. Hasegawa, M. Ishida, T. Nakajima, Y. Honda, O. Kitao, H. Nakai, T. Vreven, K. Throssell, M. J. J. A., J. E. Peralta, F. Ogliaro, M. J. Bearpark, J. J. Heyd, E. N. Brothers, K. N. Kudin, V. N. Staroverov, T. A. Keith, R. Kobayashi, J. Normand, K. Raghavachari, A. P. Rendell, J. C. Burant, S. S. Iyengar, J. Tomasi, M. Cossi, J. M. Millam, M. Klene, C. Adamo, R. Cammi, J. W. Ochterski, R. L. Martin, K. Morokuma, O. Farkas, J. B. Foresman and D. J. Fox, *Gaussian 16, Revision A. 03, Gaussian*, 2016, Gaussian, Inc., Wallingford CT, 2016.

(17) G. Karlström, R. Lindh, P. Malmqvist, B. O. Roos, U. Ryde, V. Veryazov, P.-O. Widmark, M. Cossi, B. Schimmelpfennig, P. Neogrady and L. Seijo, *Comput. Mater. Sci.*, 2003, **28**, 222–239.

(18) F. Aquilante, J. Autschbach, R. K. Carlson, L. F. Chibotaru, M. G. Delcey, L. De Vico, I. Fdez. Galván, N. Ferré, L. M. Frutos, L. Gagliardi, M. Garavelli, A. Giussani, C. E. Hoyer, G. Li Manni, H. Lischka, D. Ma, P. Å. Malmqvist, T. Müller, A. Nenov, M. Olivucci, T. B. Pedersen, D. L. Peng, F. Plasser, B. Pritchard, M. Reiher, I. Rivalta, I. Schapiro, J. Segarra-Martí, M. Stenrup, D. G. Truhlar, L. Ungur, A. Valentini, S. Vancoillie, V. Veryazov, V. P. Vysotskiy, O. Weingart, F. Zapata and R. Lindh, *J. Comput. Chem.*, 2016, **37**, 506–541.

(19) C. Zhu and H. Nakamura, *J. Chem. Phys.*, 1994, **101**, 10630–10647.

(20) C. Zhu and H. Nakamura, *J. Chem. Phys.*, 1995, **102**, 7448–7461.

(21) C. Zhu, K. Nobusada and H. Nakamura, *J. Chem. Phys.*, 2001, **115**, 3031–3044.

(22) L. Yu, C. Xu, Y. Lei, C. Zhu and Z. Wen, *Phys. Chem. Chem. Phys.*, 2014, **16**, 25883–25895.

(23) L. Yu, C. Xu and C. Zhu, *Phys. Chem. Chem. Phys.*, 2015, **17**, 17646–17660.

(24) E. Wigner, *Phys. Rev.*, 1932, **40**, 749–759.

(25) M. Barbatti, G. Granucci, M. Persico, M. Ruckenbauer, M. Vazdar, M. Eckert-Maksić and H. Lischka, *J. Photochem. Photobiol. A*, 2007, **190**, 228–240.

(26) M. Barbatti, M. Ruckenbauer, F. Plasser, J. Pittner, G. Granucci, M. Persico and H. Lischka, *Wiley Interdiscip. Rev. Comput. Mol. Sci.*, 2014, **4**, 26–33.

(27) M. Barbatti, G. Granucci, M. Ruckenbauer, F. Plasser, R. Crespo-Otero, J. Pittner, M. Persico and H. Lischka, *Version 1.4*.

(28) G. L. Cui and W. Thiel, *J. Chem. Phys.*, 2014, **141**, 124101.

(29) E. E. Dahlke and D. G. Truhlar, *J. Chem. Theory Comput.*, 2007, **3**, 46–53.